

University of California at Santa Cruz

Millikan Oil Drop

PHYS 134 Lab Report

by

Jacob Shearer

Instructor: Sasha Sher

Contents

List of Figures	iii
List of Tables	vi
1 Introduction	1
1.1 Background	3
1.2 Forces on the Droplets	4
1.3 Stage One of the Experiment	8
1.4 Stage Two of the Experiment	9
2 Methods	11
2.1 Description of Apparatus.	11
2.2 Droplet Data Collection	16
2.3 Tracking Droplet Positions With Computer Vision	17
2.4 Calculating Droplet Velocities	20
2.5 Determination of a	22
2.6 Determination of q	23
2.7 The Final Value of e	24
3 Results	27
4 Discussion	30
5 Bibliography	33

List of Figures

- 1.1 A diagram showcasing the coordinate system used during the oil drop experiment. A droplet (pictured in gray) falling inside of the main chamber of the apparatus moves in the positive y-direction, and a droplet rising moves in the negative y-direction. Only the y-direction was relevant during the analysis of the experimental data. (4)

1.2 A simplified diagram of the Millikan experiments' main chamber. Metal plates are positioned at the top and bottom of the chamber, and are therefore separated by a distance d . When the plates are charged with a high voltage power source (positively on the top plate, negatively on the bottom plate), an electric field is created inside of the chamber. This field points down from the positively charged plate to the negatively charged plate. (6)

1.3 A free body diagram of the forces experienced by a droplet during the first stage of the experiment. The droplet is pulled downwards by the force of gravity (F_g) and pushed upwards by the drag force (F_{drag}) caused by its movement through the air. After a short period of time the drag force grows so that it is the same magnitude as the gravitational force, and the droplet reaches terminal velocity (v_{y0}). (8)

1.4 A free body diagram of the forces experienced by a droplet during the second stage of the experiment. The droplet is pulled upwards by the electric force (F_E) while also being pulled/pushed downwards by the gravitational force (F_G) and the drag force (F_{drag}). As the droplet's upward velocity increases, the drag force grows to the point where the sum of the drag force and the gravitational force are equal in magnitude to that of the electric force, and the droplet once again reaches terminal velocity (V_{yE}). (9)

- 2.1 An overhead view of the apparatus used to observe and manipulate oil droplets (“PASCO,” p. 3). The apparatus is mounted on a leveling platform which is calibrated using the bubble level. Droplets are sprayed into the main chamber through a hole in the top of the droplet viewing chamber housing, and once inside they are illuminated by a halogen lamp and can thus be viewed through the scope. Droplets can be ionized using the ionization lever, and the electric field used to manipulate the droplets is toggled using the plate charging switch. Finally, the temperature inside of the chamber is monitored using a multimeter connected to a thermistor by the two connectors. (12)
- 2.2 An exploded view of the apparatus’ droplet viewing chamber (“PASCO,” p. 4). Droplets are sprayed into the chamber via the hole at the top of the lid, and depending on the position of the ionization source lever depicted in figure 2.1, droplets can be ionized via a thorium-232 alpha radiation emitter. Finally, droplets are manipulated via an electric field that results from charging the upper and lower capacitor plates with a high voltage power supply. These plates are separated by a plastic spacer of thickness d (13)
- 2.3 An annotated screenshot of a camera’s view through the apparatus’ viewing scope. Several droplets can be seen, and appear as white dots. When in focus, droplets appear as small points of light, and when unfocused they appear as simple lightly-colored bokeh. The reticle grid lines allow for the displacement of droplets to be measured, with each major reticle line (an example of which is annotated in red) being 0.5 mm in length. (15)
- 2.4 A mask of the reticle grid lines created by the droplet-tracking program. This is necessary for the interpolation later done by the program. (17)
- 2.5 A frame of droplet video with the grid line mask applied. Although the grid lines are still visible, they are nowhere near as obstructive as before because the program interpolates at the locations of the mask, filling in droplets that may have been “cut in half” by a reticle line during that particular frame and filling in the lines themselves with something resembling the background. (18)

2.6 The frame after it has been put through a binary threshold. Notice that only the droplets (the white dots) are visible now. The background is gone. This makes it very easy for the program to identify droplets. (19)

2.7 A centroid tracker is used to identify each of the droplets and apply an i.d to them so that they can be easily identified and chosen for analysis later. The position of the centroid trackers on the droplets is shown by the light green dots/squares, next to which is each of the droplets' corresponding i.d. (19)

2.8 A graph of position data for a droplet with two fit curves. The first fit curve (blue) is generated with the position of the droplet as it is falling, and by taking the slope of this curve the fall velocity can be determined. The second curve (orange) is generated with the position of the droplet as it is rising, and by taking this curve's slope the droplet's rise velocity can be determined. (21)

3.1 A plot summarizing all of the values of e calculated from charge differences between droplet runs. The uncertainties in these values are given by the orange error bars, and the commonly accepted value for e is depicted as a vertical green line. (28)

3.2 A histogram of the calculated values of e with the commonly accepted value of e (the vertical green line) displayed for reference. This histogram was generated using python's `np.hist` function automatically using a total of 100 bins. (29)

List of Tables

- | | | |
|-----|--|------|
| 2.1 | A summary of the measured pixel lengths of major reticle grid lines and their resulting mm/pixel conversions. Because the reticle lines weren't perfectly straight, pythagorean theorem was used to calculate their exact lengths in pixels using the x and y coordinates of their tops and bottoms. | (20) |
| 2.2 | A list of all the constants used in the calculation of both the radii of the droplets and the charges of the droplets. These were obtained from a table included in Brown (2022, p. 38). | (23) |
| 3.1 | A summary of the calculated charge differences between runs for each of the nine measured droplets. | (27) |

1

Introduction

In the year 1897, British physicist J.J. Thomson discovered that the rays emitted by cathode ray tubes were composed of a hitherto undiscovered particle which carried a negative charge and was of significantly smaller size than a regular atom (Shamos, 1987, p. 327). Thomson had discovered the first subatomic particle, which he called an *electron* after the name given by Irish physicist George Stoney to the indivisible quantity of electric charge used to explain the chemical properties of atoms (“PASCO,” p. 11).

Following Thomson’s discovery, several attempts were made to determine the exact charge carried by these electrons. Thomson himself first tried to measure the charge via a method involving the electrolysis of sulphuric acid. This process created a cloud of ionized gas which Thomson was able to weigh, and using this weight he was able to determine the number of ions in the cloud. With this, he simply divided the total charge of the cloud by the number of ions to obtain a charge value (“PASCO,” p. 11). H.S. Wilson, a colleague of Thomson, later employed a similar method, but with an important twist: the gas cloud was formed between two brass plates between which a potential difference, and hence an electric field, could be generated. The movement of the cloud was observed both with and without this electric field, and the velocities of the cloud in these two states were used to determine a charge value (“PASCO,” pp. 11-12).

Although these two experimental methods represented steps in the right direction, neither produced particularly accurate values for the charge of an electron. It would take American physicist Robert Millikan to measure a value for e anywhere near what is commonly accepted today. Millikan first employed a method which was quite similar to that of his predecessors: observing the behavior of water droplets within a cloud under the effects of an electric field. But later on, Millikan modified his experimental technique to instead use a higher potential across the two plates and *oil drops* instead of water droplets.

The experiment detailed in this report seeks to recreate Millikan's famous oil drop experiment and measure the charge of an electron. An atomizer is used to spray a cloud of tiny, non-volatile oil droplets between two metal plates which are capable of being charged. The behavior of each droplet is then observed in two stages. During the first stage, the droplets are allowed to free fall within the chamber, and in doing so they reach a terminal velocity. This velocity can be measured for a single droplet and used to determine its radius. During the second stage a potential difference is introduced across the aforementioned metal plates, which produces an electric field within the chamber. As a result of this field, the negatively-charged droplet will begin to rise and will again reach terminal velocity, only in the opposite direction as before. This rise velocity is measured and used in conjunction with the previously determined radius and fall velocity to calculate the charge on the drop. By measuring many different droplet charges over the course of several trials, the charge of an electron can then finally be determined.

Obtaining a value for the exact charge of an electron is of interest for a variety of reasons, with the first and foremost being that all atoms, from simple hydrogen all the way up to Oganesson, contain electrons. As negatively charged particles, electrons orbit the positively charged nuclei of atoms in fixed orbits depending on their energy and angular momentum. Even

further, all chemical reactions between atoms are a result of the ways in which they exchange, share, or lose electrons to one another. Thus, knowing the charge of the electron is crucial for modeling and understanding atoms and their chemical interactions with each other.

Aside from measuring the exact charge of an electron, though, this experiment also demonstrates an important physical phenomenon: charge quantization. Electrons are a type of fundamental particle, meaning that they cannot be divided into smaller particles. As such, they represent the smallest unit of negative electric charge found in nature. All negative electric charge found in the universe is either equal to that of an electron or is equal to some integer multiple of the electron's charge. This means that electric charge is *quantized*, or comes in finite, discrete packets. If the oil droplets observed over the course of the experiment have either a charge of e or some integer multiple of it, then we will have obtained very good evidence that charge, and possibly other quantities, are indeed quantized.

1.1 Background

Forces are the attractions or repulsions felt between objects resulting from their mutual interactions. Objects which experience a force will be accelerated in proportion to their mass and the strength of the applied force, as described by Equation 1.1, Newton's second law:

$$F = ma \quad (1.1)$$

Over the course of the experiment, oil droplets inside of the apparatus experience three forces of note: the gravitational force, drag force, and the electric force. Although the droplets only experience the first two forces during the first stage of the experiment, they experience all three during the second stage, and thus it is worthwhile to spend some time discussing each force

individually. But before doing so, it is important to understand the coordinate system used in the experiment, depicted in Figure 1.1.

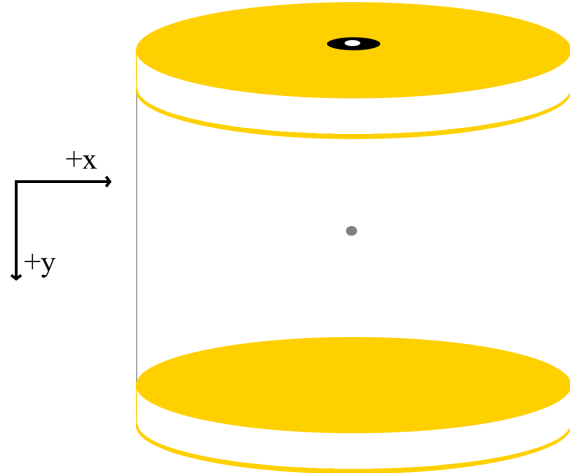


Figure 1.1: A diagram showcasing the coordinate system used during the oil drop experiment. A droplet (pictured in gray) falling inside of the main chamber of the apparatus moves in the positive y-direction, and a droplet rising moves in the negative y-direction. Only the y-direction was relevant during the analysis of the experimental data.

As the diagram shows, falling droplets move in the positive y-direction and rising droplets move in the negative y-direction, and although the droplets are free to move in all three directions, both the gravitational and electric forces are pointed along the y-axis, so only movement in the y-direction was relevant to the determination of the droplets' charges. Thus, all forces discussed here are presented in their one-dimensional forms.

1.2 Forces on the Droplets

Firstly, as objects with mass, the droplets experience a mutual gravitational attraction with the Earth. Objects near the surface of the Earth (where this experiment was performed) will

have an acceleration $g = 9.81 \text{ m/s}^2$, and thus the strength of the gravitational force experienced by the droplets is given by Equation 1.2

$$F_g = m_d g \quad (1.2)$$

where m_d is the mass of a droplet (Giancoli, 2000, p. 85). Because the masses of the droplets are difficult to determine directly, m_d can instead be calculated using Equation 1.3

$$m_d = V_d \rho = \frac{4}{3} \pi a^3 \rho \quad (1.3)$$

where V_d is the volume of a droplet with radius a and ρ is the density of the oil that the droplets are composed of. Inserting this relation into Equation 1.2 yields Equation 1.4, the strength of the gravitational force on the droplets in terms of g , a , and ρ :

$$F_g = \frac{4}{3} \pi a^3 \rho g \quad (1.4)$$

The second force that the droplets experience is a drag force, which is due to their movement through the air, a viscous medium. The strength of this force is proportional to the velocity of the droplets and is always directed opposite to their direction of motion. This is shown by Equation 1.5, Stokes law for viscous drag,

$$F_{drag} = -6\pi a v \eta_{eff} \quad (1.5)$$

where v is the velocity of the droplets, and η_{eff} is the effective viscosity of the air. The exact value for η_{eff} is given by Equation 1.6

$$\eta_{eff} = \frac{\eta_0}{1+b/pa} \quad (1.6)$$

which includes η_0 , the viscosity of air, b , the viscosity correction factor, and p , the atmospheric pressure. This term is present in Equation 1.5 to account for the fact that the effective viscosity of the air differs from the regular viscosity of the air when the radius of an oil droplet approaches

the mean free path of air molecules (“PASCO,” p. 14). Inserting this relation into Equation 1.5 yields Equation 1.7, the strength of the drag force in terms of the droplets’ velocity and other constants.

$$F_{drag} = -6\pi av \frac{\eta_0}{1+b/pa} \quad (1.7)$$

Notice that this force is *linearly proportional* to the velocity of the droplets. Although in principle the drag on an object moving through a viscous medium is both linearly and quadratically proportional to the object’s velocity, the droplets are small enough in this case that any quadratic drag can be neglected (Taylor, 2003, p. 46).

The third and final force felt by the droplets during the experiment is the electric force, which results from the droplets’ charge. As mentioned above, the apparatus creates an electric field inside of its main chamber (where the droplets are located) by charging metal plates at the top and bottom of the chamber. This is depicted in Figure 1.2, shown below:

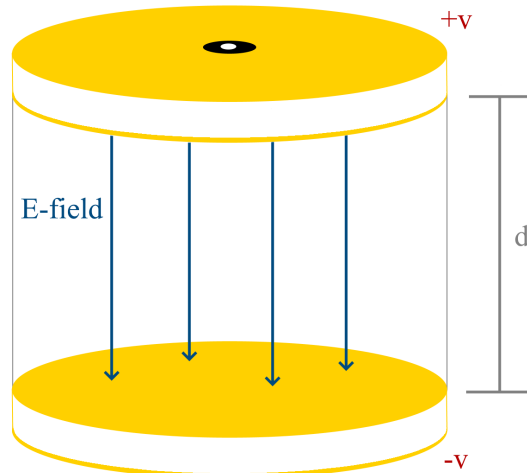


Figure 1.2: A simplified diagram of the Millikan experiments’ main chamber. Metal plates are positioned at the top and bottom of the chamber, and are therefore separated by a distance d .

When the plates are charged with a high voltage power source (positively on the top plate, negatively on the bottom plate), an electric field is created inside of the chamber. This field points down from the positively charged plate to the negatively charged plate.

As the diagram shows, the electric field results from a potential difference of V between the plates, which are separated by a distance d . The potential difference between two these plates in terms of the electric field is given by Equation 1.8

$$\Delta V = \int \vec{E} \cdot d\vec{l} \quad (1.8)$$

and because the oil drops are much smaller than the plates themselves, the electric field experienced by the droplets can be considered uniform, and thus Equation 1.8 simplifies to Equation 1.9:

$$V = \int E \cdot dl = Ed \quad (1.9)$$

Finally, the strength of the electric force is given by Equation 1.10 (Giancoli, 2000, p. 555), and solving Equation 1.9 for E and substituting it into Equation 1.10 yields Equation 1.11

$$F_E = qE \quad (1.10)$$

$$F_E = q \frac{V}{d} \quad (1.11)$$

Thus, the electric force felt by the droplets depends on the voltage across the charged plates V , the distance between the plates d (effectively the height of the chamber) and the charge on the droplets q . However, because the droplets are negatively charged, they will feel an electric force in the opposite direction of the electric field.

1.3 Stage One of the Experiment

With each of the forces experienced by the droplets explained, it's now time to examine how the droplets behave under their effects. As mentioned above, during the first stage of the experiment a droplet encounters two forces: the force of gravity and a drag force which is linearly proportional to its velocity. Figure 1.3, presented below, depicts a free body diagram of these two forces as they act on a droplet.

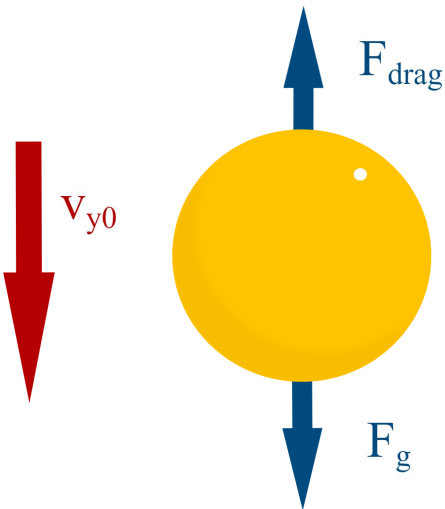


Figure 1.3: A free body diagram of the forces experienced by a droplet during the first stage of the experiment. The droplet is pulled downwards by the force of gravity (F_g) and pushed upwards by the drag force (F_{drag}) caused by its movement through the air. After a short period of time the drag force grows so that it is the same magnitude as the gravitational force, and the droplet reaches terminal velocity (v_{y0}).

The droplet is first accelerated by the force of gravity, but as its velocity increases, so does the strength of the drag force. Eventually, the gravitational and drag forces reach a point where they are equal to one another, and the droplet stops accelerating. This is described by Equations 1.12 and 1.13

$$F_g + F_{drag} = 0 \quad (1.12)$$

$$\frac{4}{3}\pi a^3 \rho g - 6\pi a v_{y0} \frac{\eta_0}{1+b/pa} = 0 \quad (1.13)$$

where Equation 1.13 is obtained by substituting Equations 1.4 and 1.7 into Equation 1.12.

It's at this stage that the droplet reaches its terminal velocity, v_{y0} , which it does in only a few milliseconds (Brown, 2022, p. 35). This velocity is relatively easy to measure, and doing so provides a convenient way to determine the radius of a droplet, a . By solving Equation 1.13 for a we obtain Equation 1.14

$$a = \sqrt{\left(\frac{b}{2p}\right)^2 + \frac{9\eta_0 v_{y0}}{2g\rho}} + \frac{b}{2p} \quad (1.14)$$

which yields the radius of a droplet in terms of known quantities.

1.4 Stage Two of the Experiment

This stage of the experiment differs from the previous one in that the droplet experiences all three forces at once. This is shown by Figure 1.4, presented below:

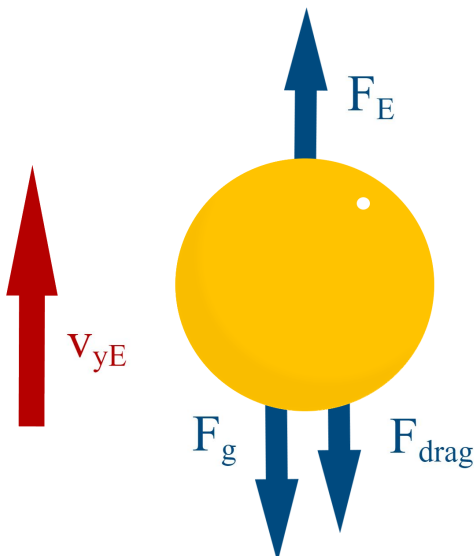


Figure 1.4: A free body diagram of the forces experienced by a droplet during the second stage of the experiment. The droplet is pulled upwards by the electric force (F_E) while also being pulled/pushed downwards by the gravitational force (F_G) and the drag force (F_{drag}). As the droplet's upward velocity increases, the drag force grows to the point where the sum of the drag force and the gravitational force are equal in magnitude to that of the electric force, and the droplet once again reaches terminal velocity (V_{yE}).

In contrast with the last stage, the droplet starts out by accelerating upwards due to the electric force. Eventually, though, its upward velocity becomes great enough that the total magnitude of the sum of the gravitational force and the drag force are equal to that of the electric force, and the droplet once again stops accelerating. This is described by Equations 1.15 and 1.16:

$$F_g + F_{drag} + F_E = 0 \quad (1.15)$$

$$\frac{4}{3}\pi a^3 \rho g - 6\pi a v_{yE} \frac{\eta_0}{1+b/pa} + q \frac{V}{d} = 0 \quad (1.16)$$

Where Equation 1.16 was obtained by plugging Equations 1.4, 1.7, and 1.11 into Equation 1.15.

As with the previous stage of the experiment, the droplet once again reaches terminal velocity (v_{yE}), though this time in the opposite direction as before. Measuring this velocity will allow us to calculate the charge on the droplet, q . Via a system of Equations 1.13 and 1.16, we obtain Equation 1.17

$$q = \frac{4}{3}\pi a^3 \rho g \frac{d}{V} \frac{v_{yE} - v_{y0}}{v_{y0}} \quad (1.17)$$

which gives the charge of the droplet in terms of its radius, a , its falling terminal velocity, v_{y0} , and its rising terminal velocity, v_{yE} (Brown, 2022, p. 37).

2

Methods

Using an atomizer, a cloud of charged droplets was sprayed into the main chamber of the apparatus, and out of this cloud a particular droplet was picked for measurement. The droplet was first allowed to fall inside of the chamber before an electric field was activated which made the droplet rise. All measured droplets were allowed to fall and rise three times, yielding three fall and rise velocities, and for each run a droplet's radius and charge were calculated using these velocities. Comparing the charges for a given droplet between runs yielded two values for e , and conducting a weighted average with all of these values yielded the final e value.

2.1 Description of Apparatus

Figure 2.1, presented below, depicts an overhead view of the apparatus used for this experiment.

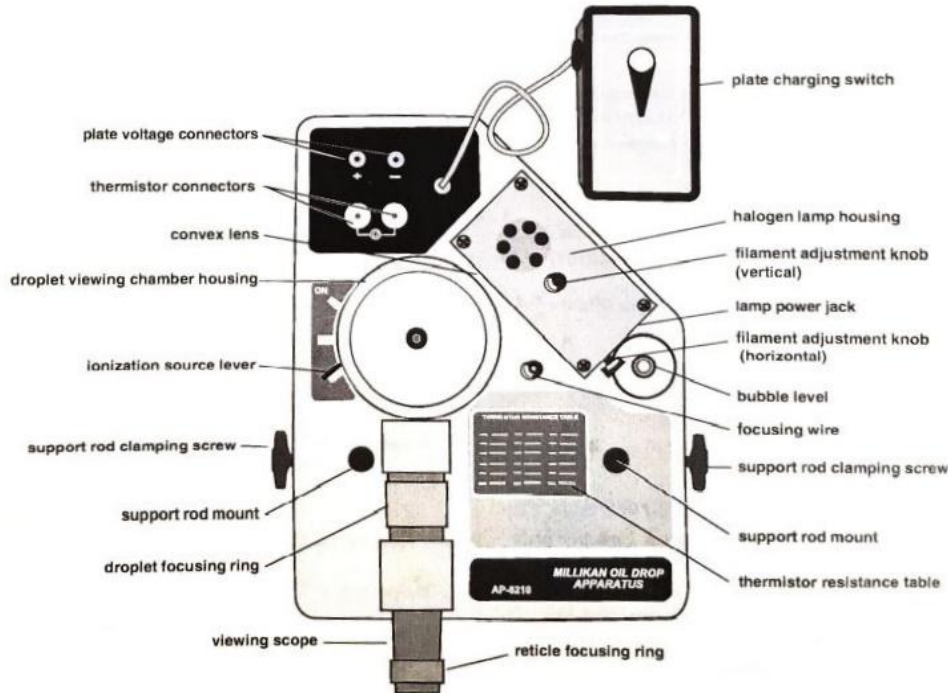


Figure 2.1: An overhead view of the apparatus used to observe and manipulate oil droplets (“PASCO,” p. 3). The apparatus is mounted on a leveling platform which is calibrated using the bubble level. Droplets are sprayed into the main chamber through a hole in the top of the droplet viewing chamber housing, and once inside they are illuminated by a halogen lamp and can thus be viewed through the scope. Droplets can be ionized using the ionization lever, and the electric field used to manipulate the droplets is toggled using the plate charging switch. Finally, the temperature inside of the chamber is monitored using a multimeter connected to a thermistor by the two connectors.

Additionally, Figure 2.2 depicts an exploded view of the droplet viewing chamber itself.

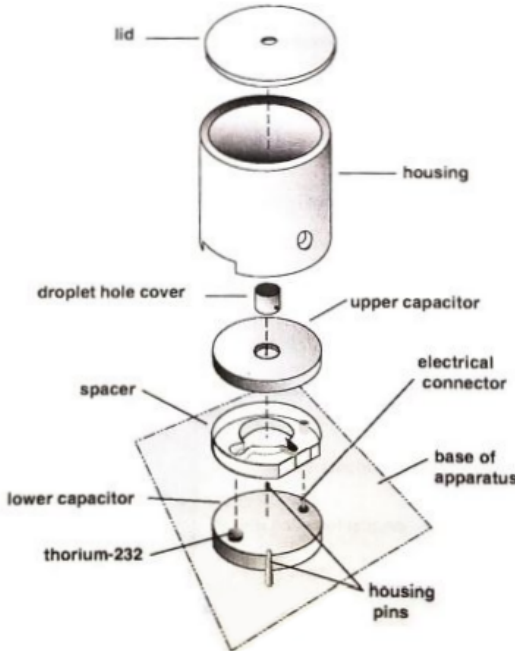


Figure 2.2: An exploded view of the apparatus' droplet viewing chamber (“PASCO,” p. 4). Droplets are sprayed into the chamber via the hole at the top of the lid, and depending on the position of the ionization source lever depicted in figure 2.1, droplets can be ionized via a thorium-232 alpha radiation emitter. Finally, droplets are manipulated via an electric field that results from charging the upper and lower capacitor plates with a high voltage power supply. These plates are separated by a plastic spacer of thickness d .

As figure 1.1 shows, the apparatus is essentially just a platform with a lamp, a droplet viewing chamber, a viewing scope, and several electrical connectors mounted to it.

The platform itself is attached to a leveling mount that is adjusted using the built-in bubble level. This is done so that the gravitational and electric forces felt by the droplet are directed along the y-axis of our coordinate system. Droplets are sprayed inside of the viewing chamber and, once inside, are illuminated by a halogen lamp and can be viewed through the scope. Two connectors seen at the top of the apparatus allow for a high voltage power supply to be connected to the plates of the viewing chamber, and a plate charging switch allows for toggling of the charge on the plates. And finally, connecting a multimeter to the thermistor

connectors at the top of the apparatus and comparing the measured resistance with the table at the apparatus' bottom right corner allows the temperature inside of the chamber to be monitored.

Of all these components, the most important part of the apparatus is the droplet viewing chamber, where the droplets can be observed falling and rising. As depicted in Figure 2.2, the chamber consists of two capacitor plates separated by a plastic spacer with a hole in the middle, all of which is contained inside of a housing. The plates are thus separated by a distance equal to the thickness of the plastic spacer, 7.53 ± 0.01 mm, which was measured by disassembling the chamber and measuring the spacer with a pair of dial calipers. As mentioned above, the capacitor plates can be charged with a high voltage power supply (500 volts) which is toggleable via the plate charging switch. There are three settings: *off* (plates are grounded), *positive* (top plate is positively charged), and *negative* (top plate is negatively charged). In this experiment, the first two settings were those used the most often.

The droplets are sprayed into the chamber using an atomizer, and thus are usually charged by friction (Shamos, 1987, p. 357). However, droplets can also be ionized using a small bit of thorium-232 isotope, which is an alpha (ionizing) radiation emitter. The ionization source lever, depicted in Figure 2.1, has three settings. The first lever setting is *off*, under which the ionization source is covered in plastic which blocks its emissions. The second setting is *spray*, which blocks the ionization source and opens a small hole in the bottom of the chamber, allowing air to escape. This setting is useful when droplets are being sprayed into the chamber, as it prevents sprayed air from bouncing off of the bottom of the chamber and creating turbulent air currents which could blow the droplets around. The final setting, *on*, simply retracts the plastic blocking the source, allowing it to ionize the droplets.

Once the droplets are inside of the chamber, they are illuminated by a halogen lamp through a small hole in the chamber housing, which makes them appear quite bright against the fairly dark background. This makes it easy to see the droplets through the viewing scope, which contains a reticle for measuring the displacement of the droplets directly and a focus ring so that particular droplets can be more easily isolated. Additionally, although it is not pictured in the figures, a camera was positioned such that it could record the inside of the chamber through the scope. The camera was able to record 1080p resolution, 5 fps video clips, and an annotated screenshot of its view through the scope is depicted in Figure 2.3:

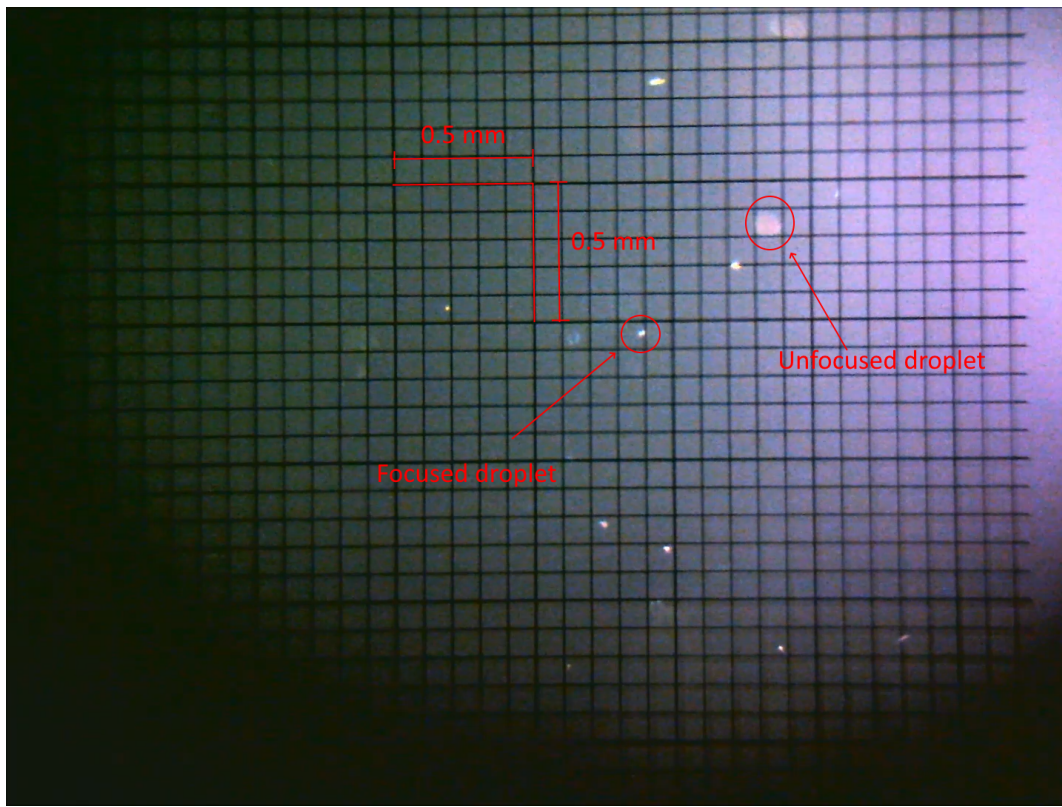


Figure 2.3: An annotated screenshot of a camera's view through the apparatus' viewing scope. Several droplets can be seen, and appear as white dots. When in focus, droplets appear as small points of light, and when unfocused they appear as simple lightly-colored bokeh. The reticle grid lines allow for the displacement of droplets to be measured, with each major reticle line (an example of which is annotated in red) being 0.5 mm in length.

As the figure shows, droplets are seen through the view as white points of light against the fairly dark background, which made them much easier to track with the software which will be discussed later in this section.

2.2 Droplet Data Collection

Droplet data is collected by first spraying oil into the droplet viewing chamber using an atomizer. As mentioned above, while the atomizer bulb is being squeezed the ionization source lever is set to *spray* to ensure that sprayed air doesn't bounce off of the bottom of the chamber and blow droplets out of view. After the spraying is over, a particular droplet is selected for measurement, and once this droplet reaches one of the major reticle lines the recording with the camera begins.

The droplet is then allowed to fall, and as it falls the ionization lever is then set to its *on* position for about five seconds, which ionizes the droplet. Once the droplet reaches another one of the major reticle lines the plate charging switch is toggled, creating a positive charge on the top capacitor plate and a negative one on the bottom plate. The resulting electric field inside the chamber causes the droplet to rise, which it is allowed to do until it reaches the starting major reticle line. Upon reaching this point, the electric field is switched back off and the process restarts. In total, the droplet is allowed to rise and fall in this manner three times. Once it has done so, the recording is ended and collection is completed. This process was repeated for each of the droplets, resulting in 3 rises and falls per droplet.

2.3 Tracking Droplet Positions With Computer Vision

Although it would've been possible to simply measure the positions of the droplets using the reticle depicted in Figure 2.3, using computer software to track their positions proved to be a more accurate, and less uncertain, way of doing so. To accomplish this, a custom program was written in python using the openCV library, which contains many methods and functions which are optimized for image and video processing. The program itself is fairly complex, but the following is the general procedure that it uses to track droplets.

First, recordings made by the camera are made into grayscale. This is done for several reasons, with the primary one being that it makes the droplets easier for the program to recognize. But doing so also makes the video processing by the program faster and reduces the complexity of the code, among other things. After this is done, a mask is made of the reticle grid lines seen in the recording, as shown in Figure 2.4:

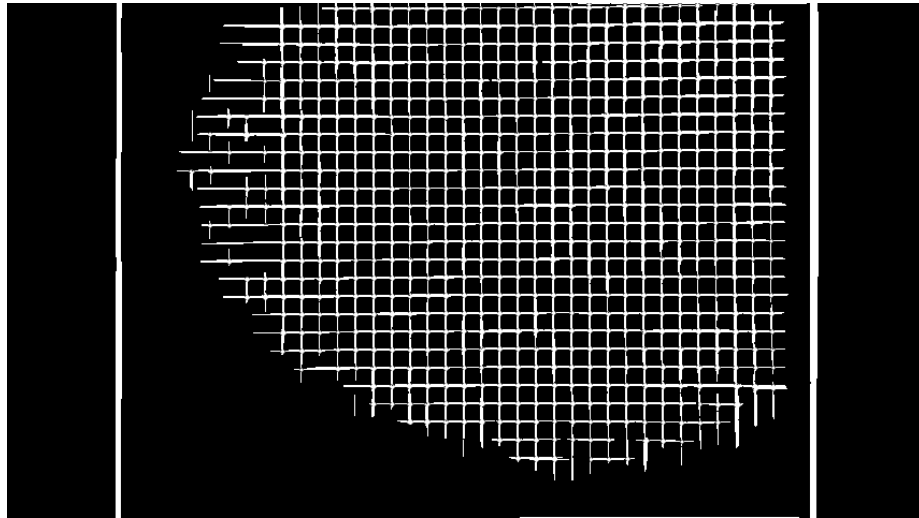


Figure 2.4: A mask of the reticle grid lines created by the droplet-tracking program. This is necessary for the interpolation later done by the program.

This mask makes it possible to “screen out” the grid lines seen in the recording to a degree, making the droplets easier for the program to track.

After the mask has been created, the program then applies it to the frame currently being analyzed. An example of this can be seen in Figure 2.5.

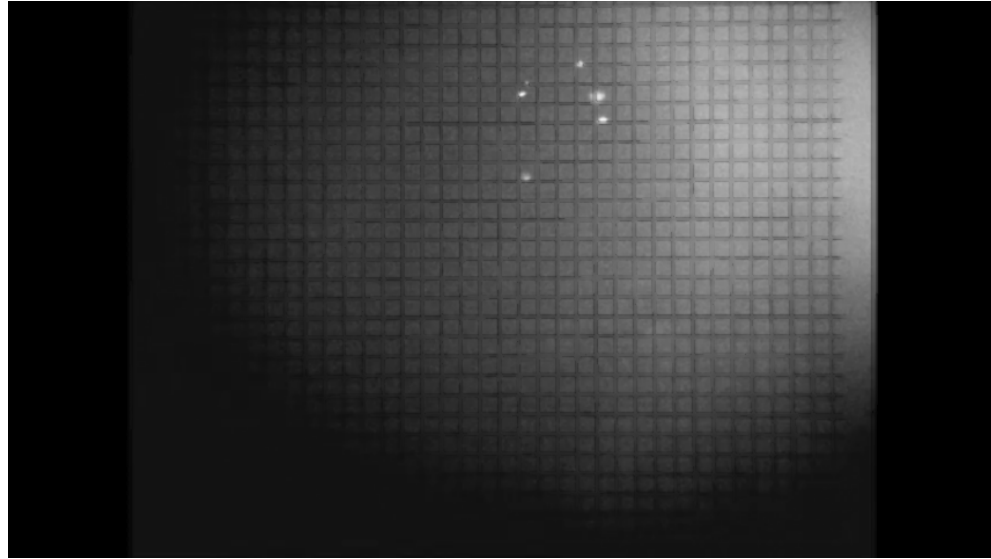


Figure 2.5: A frame of droplet video with the grid line mask applied. Although the grid lines are still visible, they are nowhere near as obstructive as before because the program interpolates at the locations of the mask, filling in droplets that may have been “cut in half” by a reticle line during that particular frame and filling in the lines themselves with something resembling the background.

By applying the mask, the grid lines become much less discernible. This, combined with some interpolation of the areas affected by the mask, helps to make the droplets easier for the program to identify. Droplets which have been “cut in half” in a particular frame are partially filled in by the interpolation process, which makes tracking on droplets more consistent.

After this, the frame is put through a binary threshold, which reduces it to black and white, as depicted in Figure 2.6:

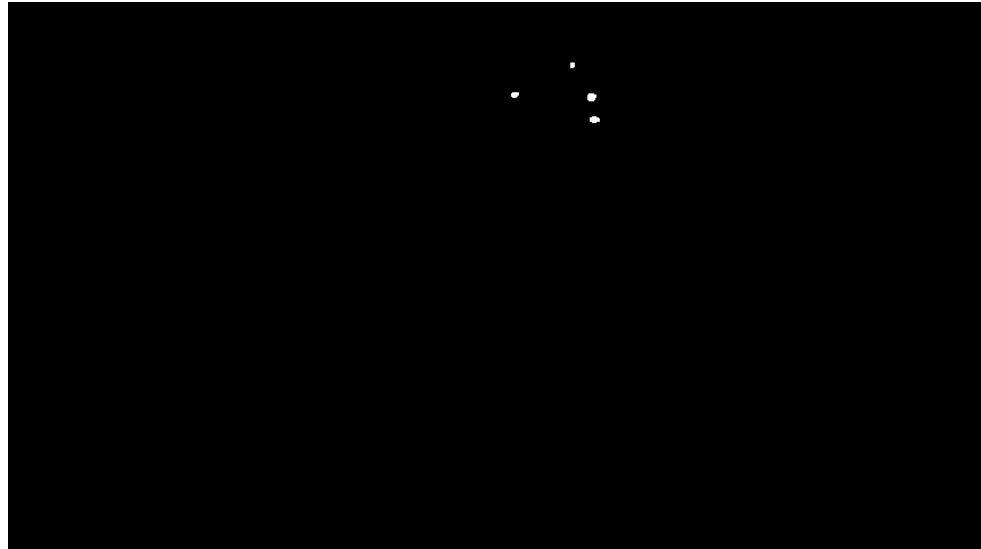


Figure 2.6: The frame after it has been put through a binary threshold. Notice that only the droplets (the white dots) are visible now. The background is gone. This makes it very easy for the program to identify droplets.

This leaves only the droplets visible, and at this point a centroid tracker is used to identify each droplet and apply an i.d to it, as shown by Figure 2.7:

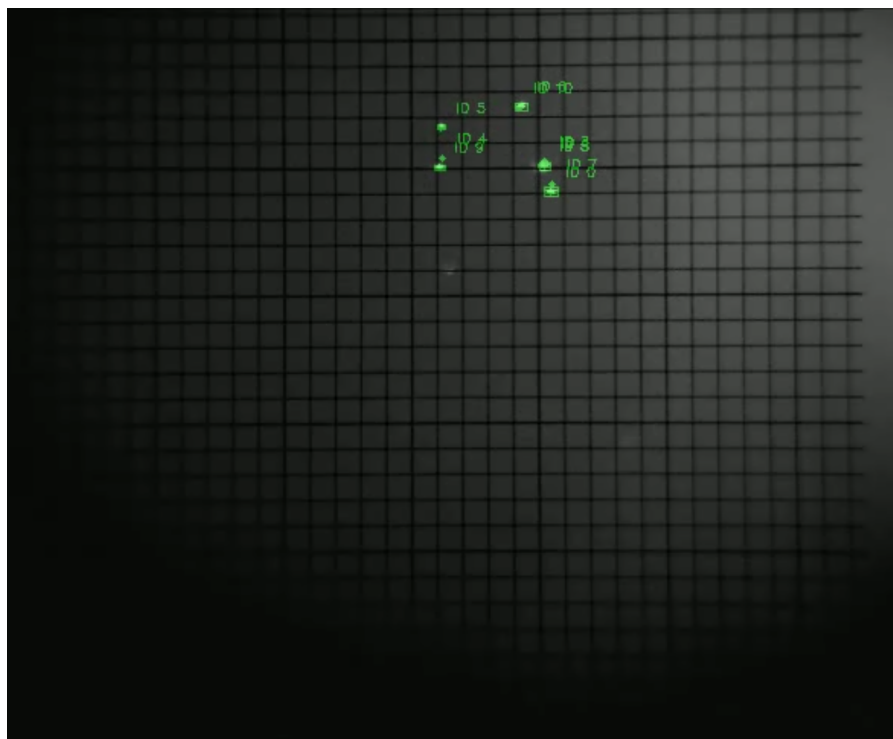


Figure 2.7: A centroid tracker is used to identify each of the droplets and apply an i.d to them so that they can be easily identified and chosen for analysis later. The position of the centroid

trackers on the droplets is shown by the light green dots/squares, next to which is each of the droplets' corresponding i.d.

Once a droplet has been identified by the centroid tracker, it can be tracked from frame to frame and can be easily picked out for analysis later.

Once this entire process has been repeated for each frame of video, the i.d of the droplet of interest can be entered into the program and its y-positions in pixels, each with an uncertainty of 1 pixel, will be returned.

2.4 Calculating Droplet Velocities

To obtain velocities from the positions of a droplet tracked by the program, they are first converted into meters using the conversion factor c , $2.72805 \times 10^{-6} \pm 6.9853 \times 10^{-8}$ m/pixel, which was obtained using a pixel measurement tool with one of the droplet video frames. Three different major reticles (of length 0.5mm) were measured, and the lengths measured in pixels were then used with Equation 2.1.

$$\text{mm/pixel} = \text{pixels}/0.5 \text{ mm} \quad (2.1)$$

Table 2.1, presented below, summarizes the pixel values and the result of Equation 2.1 for each measurement.

Pixels	mm/pixel
176.886515	0.0028266711
187.0037412	0.0026737433
186.3068698	0.0026837443

Table 2.1: A summary of the measured pixel lengths of major reticle grid lines and their resulting mm/pixel conversions. Because the reticle lines weren't perfectly straight, pythagorean theorem was used to calculate their exact lengths in pixels using the x and y coordinates of their tops and bottoms.

All three of these values were then averaged and converted to meters to obtain the conversion factor. The uncertainty in the conversion factor was obtained by taking the standard deviation of these values and converting that to meters as well.

With this conversion in hand, y-positions and their uncertainties can be converted from pixels to meters using Equations 2.2-2.4

$$y_c = yc \quad (2.2)$$

$$\sigma_{y_c} = \sqrt{(\sigma_y \frac{dy_c}{dy})^2 + (\sigma_c \frac{dy_c}{dc})^2} \quad (2.3)$$

$$\sigma_{y_c} = \sqrt{(\sigma_y c)^2 + (\sigma_c y)^2} \quad (2.4)$$

where y_c is the position in meters, c is the conversion factor, and Equation 2.4 was obtained by evaluating the derivatives of Equation 2.3.

Finally, with all of the droplet's positions in meters, the function `scipy.optimize.curve_fit` is used to calculate the slope (and its uncertainty) of the positions over a given range. A graphical example of this is given in Figure 2.8, presented below.

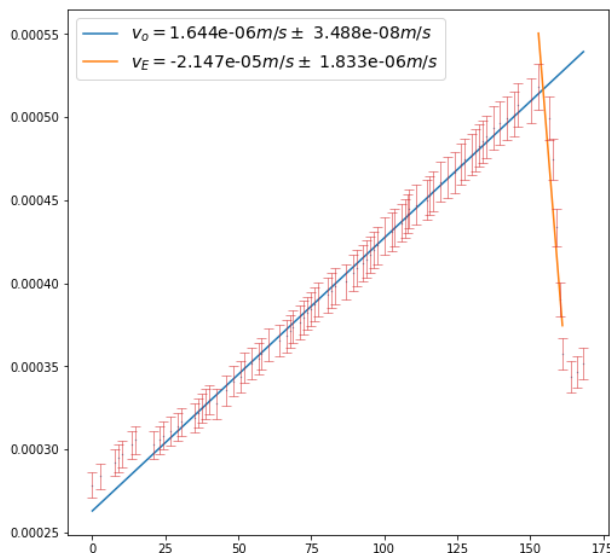


Figure 2.8: A graph of position data for a droplet with two fit curves. The first fit curve (blue) is generated with the position of the droplet as it is falling, and by taking the slope of this curve the fall velocity can be determined. The second curve (orange) is generated with the position of the droplet as it is rising, and by taking this curve's slope the droplet's rise velocity can be determined.

As the figure above shows, the positions are split into two ranges, each with its own slope. If these ranges are chosen correctly, the calculated slopes and their uncertainties are simply the desired fall or rise velocities and their corresponding uncertainties.

2.5 Determination of a

With the fall velocities obtained via the procedure described in the previous section, the radii of the droplets can be calculated using Equation 1.14, restated here.

$$a = \sqrt{\left(\frac{b}{2p}\right)^2 + \frac{9\eta_0 v_{y0}}{2g\rho}} + \frac{b}{2p} \quad (1.14)$$

The uncertainty in this value is given by Equation 2.5, the error propagation of Equation 1.14.

$$\sigma_a = \sqrt{\left(\frac{da}{dv_{y0}}\sigma_{v_{y0}}\right)^2} \quad (2.5)$$

Evaluating the derivative in this equation and simplifying yields Equation 2.6

$$\sigma_a = \sqrt{\frac{(\gamma\sigma_{v_{y0}})^2}{4(\alpha^2 + \gamma v_{y0})}} \quad (2.6)$$

Where $\alpha = \frac{b}{2p}$ and $\gamma = \frac{9\eta_0}{2\rho g}$.

Additionally, Table 2.2 presents all of the tabulated constants used during both the droplet radius calculation and the droplet charge calculation described in the next section:

Symbol	Value	Units	Description
b	8.20E-3	N/m	Viscosity correction factor
g	9.80	m/s ²	Gravitational acceleration
p	1.013E5	N/m ²	Atmospheric pressure
V	500	Volts	Plate voltage
η_0	1.824E-5	Ns/m ²	Normal viscosity of air
ρ	8.86E2	kg/m ³	Density of oil droplets
e_{lit}	1.602E-19	C	Fundamental Charge

Table 2.2: A list of all the constants used in the calculation of both the radii of the droplets and the charges of the droplets. These were obtained from a table included in Brown (2022, p. 38).

2.6 Determination of q

Similarly to the previous subsection, the values of q for the droplets can be determined using the fall and rise velocities, as well as the previous determined values of a , with Equation 1.17, restated here.

$$q = \frac{4}{3} \pi a^3 \rho g \frac{d}{V} \frac{v_{yE} - v_{y0}}{v_{y0}} \quad (1.17)$$

The uncertainty in q is given by Equation 2.7, the error propagation of Equation 2.7.

$$\sigma_q = \sqrt{\left(\frac{dq}{da}\sigma_a\right)^2 + \left(\frac{dq}{dd}\sigma_d\right)^2 + \left(\frac{dq}{dv_{yE}}\sigma_{v_{yE}}\right)^2 + \left(\frac{dq}{dv_{y0}}\sigma_{v_{y0}}\right)^2} \quad (2.7)$$

Evaluating the derivatives in this equation yields Equation 2.8, the final uncertainty in q ,

$$\sigma_q = \sqrt{term1^2 + term2^2 + term3^2 + term4^2} \quad (2.8)$$

$$term1 = 3\sigma_a \phi a^2 d \left(\frac{v_{yE}}{v_{y0}} - 1 \right)$$

$$term2 = \sigma_d \phi a^3 \left(\frac{v_{yE}}{v_{y0}} - 1 \right)$$

$$term3 = \sigma_v \phi a^3 d \left(\frac{1}{v_{y0}} - 1 \right)$$

$$term4 = \sigma_{v_{y0}} \phi a^3 d \left(\frac{v_{yE}}{v_{y0}^2} + 1 \right)$$

where $\phi = \frac{4\pi\eta g}{3V}$.

2.7 The Final Value of e

As discussed in section 2.2, each droplet was allowed to rise and fall for a total of three runs: each with one rise and fall period. Because of this, each droplet has three associated charges, one from each run. Droplets were ionized at the beginning of each of these runs, meaning that in many cases the charge on the droplet differed from run to run slightly, and because charge is quantized this charge difference is some integer multiple of e . Thus, by computing the charge differences, a value for e can be determined.

For each droplet, the first and second runs were compared with one another, and the second and third runs were compared with one another. Charge differences between these runs were computed with Equation 2.9, and the uncertainty in the charge differences was computed with Equation 2.10

$$q_d = q_2 - q_1 \quad (2.9)$$

$$\sigma_{q_d} = \sqrt{\sigma_{q_2}^2 + \sigma_{q_1}^2} \quad (2.10)$$

where Equation 2.10 was determined through error propagation of Equation 2.9. Comparing each run with only run directly before it meant that each droplet yielded a set of two charge differences.

Once the charge differences had been computed for all of the droplets, each was divided by the known value of e , yielding a number which was then rounded to its nearest whole number. This was taken to be the integer multiple of e for each charge difference. Dividing each of the charge differences, and their uncertainties, by their corresponding integer values then yielded many values of e , as described by Equations 2.11 and 2.12:

$$e_i = q_{d_i}/n_i \quad (2.11)$$

$$\sigma_{e_i} = \sigma_{q_i}/n_i \quad (2.12)$$

These e values were then used in a weighted average to calculate the final value for e . This is described by equations 2.13 and 2.14:

$$e = \frac{\sum e_i / \sigma_{e_i}^2}{1 / \sum \sigma_{e_i}^2} \quad (2.13)$$

$$\sigma_e = \sqrt{\frac{1}{\sum \sigma_{e_i}^2}} \quad (2.14)$$

Once obtained, the final value of e was compared to the commonly accepted value of e by computing its Z-score. This was done via Equation 2.15

$$Z = \frac{e_{lit} - \bar{e}}{\sigma_{\bar{e}}} \quad (2.15)$$

where e_{lit} is the commonly accepted value of e . Finally, to determine the statistical significance of our final value for e , the two-tailed Gaussian p-value was calculated. This was done using Scipy's cumulative distribution function method and the Z-score obtained above. A significance level of 0.05 (5%) was used in this analysis.

3

Results

Out of the 25 droplet trials performed, a total of nine droplets were “good” droplets—meaning that they were well behaved and could be reliably tracked by the program described in methods—and were subsequently used in the determination of e . Measuring each of these nine droplets yielded a total of 27 rise and fall velocities, which were then used to calculate 27 different droplet radii and 27 different droplet charges. Comparing these charges using the procedure outlined in Methods yielded 18 charge differences, which are presented below in Table 3.1. Also presented is the integer associated with each charge difference.

Charge Difference (C)	Uncertainty (C)	Integer
-4.81326E-19	2.25379E-19	3
-2.97722E-18	3.54558E-19	18
-6.84834E-19	1.58535E-19	4
-7.22701E-21	1.27083E-19	1
-1.78599E-19	2.56648E-19	1
-2.97340E-19	7.84055E-20	1
-4.95001e19	7.27178E-20	3
-3.52673E-20	2.98084E-20	1
-3.67006E-20	7.73613E-20	1
-1.10620E-19	3.46683E-20	1

-2.09004E-19	1.82477E-20	1
-1.37566E-20	5.89554E-20	1
-5.86650E-20	8.74051E-20	1
-2.73894E-19	8.10763E-20	1
-7.11309E-20	9.63888E-20	1
-2.75044E-19	8.75078E-20	1
-2.59127E-19	3.13679E-20	1
-3.49085E-19	3.99957E-20	2

Table 3.1: A summary of the calculated charge differences between runs for each of the nine measured droplets.

By dividing each of these charge differences by their corresponding integer, 18 different values for e were obtained. Figure 3.1 displays all of these values, along with their associated uncertainties, in comparison with the commonly accepted value of e .

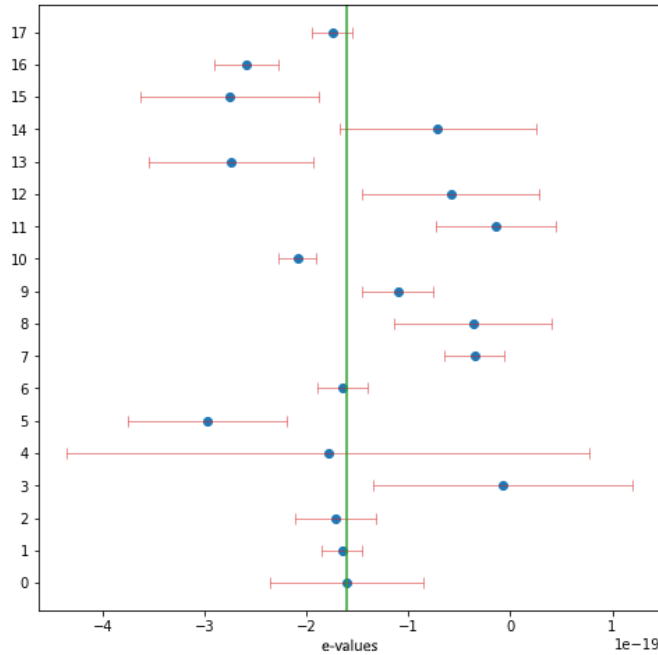


Figure 3.1: A plot summarizing all of the values of e calculated from charge differences between droplet runs. The uncertainties in these values are given by the orange error bars, and the commonly accepted value for e is depicted as a vertical green line.

Additionally, Figure 3.2 shows a histogram of these e values.

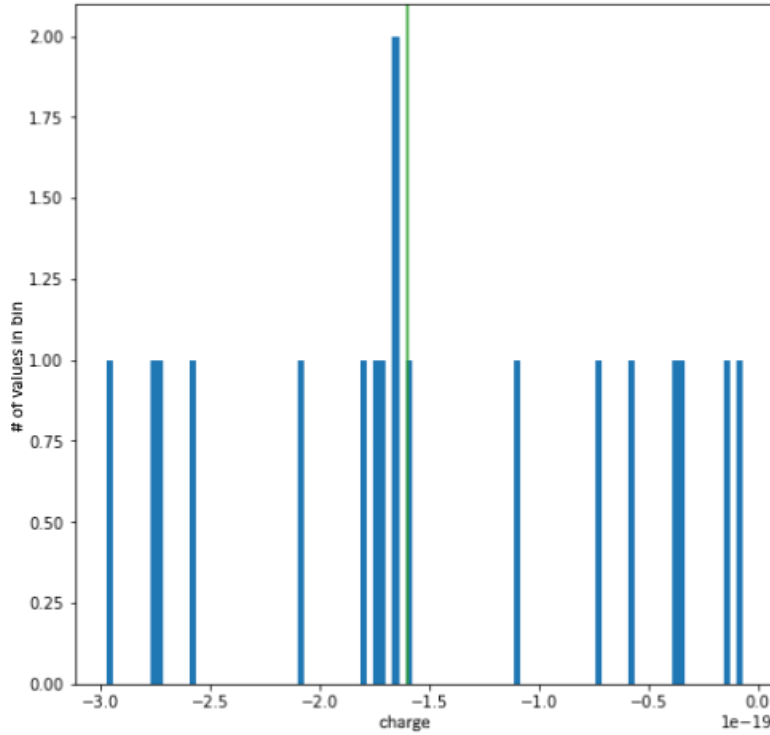


Figure 3.2: A histogram of the calculated values of e with the commonly accepted value of e (the vertical green line) displayed for reference. This histogram was generated using python's *np.hist* function automatically using a total of 100 bins.

All of these e values were then used in a weighted average described by Equations 2.13 and 2.14, which yielded the final value of e .

$$e = -1.66254 \times 10^{-19} \pm 8.22373 \times 10^{-21} \text{ Coulombs}$$

Using this value with Equation 2.15 yielded a Z-score of 0.73397, which essentially means that the final value of e is 0.734 standard deviations away from the commonly accepted value of e .

Finally, using this Z-score, the two-tailed Gaussian p-value was calculated to be 0.46296. This is greater than the significance level of 0.05, indicating that our result is consistent with the expected value.

4

Discussion

Over the course of 25 trials, 9 good droplets were measured and, via the analysis process described in the previous sections, the charge of an electron was measured to be

– 1.66254×10^{-19} ± 8.22373×10^{-21} Coulombs. This final value, as well as its uncertainty, were determined through a weighted average of the many different values of e computed from each droplet. As discussed at the end of the previous section, this result is about 0.734 standard deviations away from the commonly accepted value of e , – 1.60218×10^{-19} coulombs (NIST, 2018). And finally, our value for e , as proven by a two-tailed Gaussian p-value of approximately 0.46, is consistent with the commonly accepted value of e .

Our result for e is quite encouraging because, above all, it demonstrates the efficacy of this method for measuring the charge of an electron. Though our value for e doesn't perfectly align with the commonly accepted value, it is quite close, which suggests that at the very least this method is quite consistent. More importantly, though, is the fact that we observed quantization of charge during the experiment, just as Millikan did. As seen in the results, the measured charge differences were all roughly integer multiples of our final measured value, and this is a good indicator that charge is indeed quantized.

Even considering all of that, though, there are some ways that this experiment could be improved. To start, we could've been better about monitoring the temperature inside of the main

chamber using the thermistor. Over the course of the experiment, but especially after data collection had been going for a while, a droplet would occasionally change size in the middle of a trial due to evaporation. Keeping the halogen lamp on constantly led to a heat buildup in the chamber which, after some time, led to some slight evaporation in the droplets, and this could've been easily avoided had we monitored the temperature inside of the chamber more carefully and kept the lamp turned off in between trials. Another (and admittedly lazier) solution to this problem would've been to simply replace the halogen lamp with something like an LED that wouldn't generate as much heat under continuous use, thus eliminating the need to check the temperature entirely.

Furthermore, there are two changes that could've been made to the apparatus itself that would've made droplet measurements much easier and accurate: using a camera with a higher framerate to record the droplets and removing the reticle inside of the viewing scope. Although the camera was capable of recording videos in very high resolution (4k), it could only record five frames per second, meaning that the exact position of the droplets could only be measured every 0.2 seconds. Using a camera with a higher frame rate capability would have improved the precision of the droplets' velocity measurements and, resultantly, the precision of our final value.

Additionally, removing the reticle grid inside of the viewing scope would've made it easier for our droplet tracking program to identify droplets and measure their positions. The grid often partially blocked droplets from view for short periods, which made it harder for the program to track them from frame to frame. In retrospect, removing the reticle grid—or, at least, adjusting its focus so that it was less visible—would've been quite simple and helpful to our final result. This change not only would've made it easier for the program to track droplets, but also would've eliminated the need to engage in the extensive masking described in Methods.

The final, and most important, change would've been to simply record more droplets. Unfortunately, a great deal of our allotted time for this experiment was spent developing the droplet-tracking program, which didn't leave as much time for actual data collection. The total number of measured droplets, nine, is quite disappointing, and ideally we would've liked to have measured a number of droplets closer to four times that amount. This change, above all the others, probably would've brought about the greatest improvement, as more information could only have led to a better result.

5

Bibliography

Brown, G. (2022). *Physics 134 Lab Manual*, 35 - 38.

Giancoli, D. (2000). *Physics for Scientists and Engineers* (Vol. 3), 85, 555. Pearson.

NIST. (2018). *Elementary Charge*. Codata value. Retrieved June 4, 2022, from

<https://physics.nist.gov/cgi-bin/cuu/Value?e>

Shamos, M. H. (1987). *Great Experiments in Physics*, 327, 357. Dover Publications.

Taylor, J. R. (2003). *Classical Mechanics*, 46. University Science Books.

Unknown. *PASCO Scientific Millikan Oil Drop Apparatus Manual*.